



Accelerated Permafrost Degradation in the Source Area of the Yellow River: Spatiotemporal Dynamics of Freeze—Thaw Indices Revealed by High-Resolution DEM-Corrected ERA5-Land Data (1981–2020)

Hongying Li¹, Yingying Cui¹, Shengzhen Wang ¹, Yang Yang¹, Qiang Zhou², Fenggui Liu^{2*}, Chaorong Chen¹

¹Qinghai Provincial Key Laboratory of Plateau Climate Change and Corresponding Ecological and Environmental Effects, Qinghai Institute of Technology, Xining 810016, China

² School of National Safety and Emergency Management, Qinghai Normal University, Xining, Qinghai, 810016, China *Correspondence to*: Liu Fenggui (liufenggui@igsnrr.ac.cn)

Abstract. Permafrost degradation in the Source Area of the Yellow River (SAYR) has intensified under climate warming. Yet, the spatiotemporal patterns of freeze–thaw (F-T) dynamics remain poorly understood due to the limited availability of high-resolution data. Here, we integrate ERA5-Land reanalysis with a Digital Elevation Model (DEM) to develop a 1 km-resolution monthly surface temperature dataset (1981–2020), corrected for topographic bias using elevation-dependent temperature lapse rates. Based on this dataset, we calculate F-T indices (freezing/thawing index, thaw duration) and analyze their trends. Results show DEM correction significantly improves temperature accuracy (RMSE = 1.22° C, ubRMSE = 0.38° C). Over 40 years, air and surface freezing indices declined by -100.43 and -141.85° C·d/10a, while thawing indices increased by 83.74 and 98.47° C·d/10a, respectively. Thaw duration extended by 1.17 days/decade, with stronger trends in low-elevation zones. Freeze–thaw ratios (N-factor) exceeded 1 across all sites, indicating accelerated permafrost degradation. Spatial heterogeneity reveals thaw dominance in southeastern valleys (N > 5) versus residual freezing capacity in northwestern highlands (N < 2), driven by altitude and vegetation insulation. This study provides the first long-term, high-resolution F-T dataset for SAYR, demonstrating that topo-climatic gradients and vegetation feedbacks critically regulate permafrost stability. Our findings advance regional permafrost modeling and inform infrastructure resilience strategies in the context of climate change.

1 Introduction

The Yellow River headwaters are located in the southeastern part of the Qinghai-Tibetan Plateau (average elevation >4000 m), which is a transition zone between perennial and seasonal permafrost. As a high-temperature permafrost zone on the Tibetan Plateau (UNEP; Cheng et al. 2019), its permafrost is characterized by high temperature, thin thickness, and poor stability (Luo et al. 2012), and is highly sensitive to global warming-the warming rate has reached 0.61°C/10a since 2000, which is much higher than the average level of the Tibetan Plateau (Liu et al. 2021; Jin et al. 2022), leading to accelerated degradation





phenomena such as earlier thawing of permafrost, shorter duration of freezing, increased thickness of the active layer, and increased frequency of freezing and thawing (Zhao et al. 2020; Qin et al. 2020). These changes affect the ecological security of the region through hydrological composition, carbon cycle, and vegetation succession(Wang et al. 2022a; Jin et al. 2022; Ge et al. 2024; Piao et al. 2019), and even disrupt the Asian monsoon system (IPCC 2021; Qin et al. 2020). The accelerated permafrost degradation pattern in the Yellow River headwaters is similar to the Arctic permafrost tipping point (Douglas et al. 2021), highlighting the importance of ecological early warning for the mid-latitude permafrost region under global warming. And finally, the lack of high-precision datasets with long time series: the existing monitoring of the freeze—thaw index is mostly limited to short time series (<20 years) or coarse resolution (>10 km) (Gao et al. 2023; Ge et al. 2024; Wang et al. 2018), which limits the distribution of permafrost for climate feedback simulation and assessment. Modeling and climate feedback assessment.

Therefore, this study constructs the first 1-km resolution monthly surface temperature dataset (1981-2020) in the Yellow River headwater area by integrating the ERA5 land reanalysis data with the high-resolution DEM and overcomes the problem of topographic bias correction (RMSE reduction of 46-92%). On this basis, we systematically quantify the spatial and temporal evolution trends of freezing/thawing indices, thawing ratio, and duration of thawing period, and analyze the regulation mechanism of freezing/thawing differentiation by elevation and vegetation. The major innovations of this study include: (1) the introduction of an elevation temperature lapse rate correction model, which improves the accuracy of surface temperature estimation in complex terrain; (2) the construction of a 40-year long-series, high-resolution freeze—thaw dynamics dataset, which fills the gap of monitoring at the regional scale; and (3) the analysis of the mechanism, which systematically quantifies the nonlinear coupling between freeze—thaw variations and terrain-vegetation factors.

2 Data and methods

50 2.1 Study area

The source area of the Yellow River (SARY) is located in the northeastern part of the Qinghai-Tibetan Plateau (Figure 1), between the Bayan Kra Mountains and the Animachin Mountains in the southeastern part of Qinghai Province. The area's geomorphology is complex and diverse. It is dominated by plateau flatlands, mountains, hills, terraces, and lake basins. The topography is high in the west and low in the east. The average elevation ranges from 4,100 to 4,600 meters (Liu and Huang, 2020). The SARY is a large area of continuous, discontinuous, and seasonal permafrost. As part of the "Roof of the World" Tibetan Plateau, the SAYR has a typical inland alpine climate, with an annual mean temperature ranging from -1.67 to 1.38°C, an annual precipitation range of 447 to 702 mm, and an annual evaporation range of 1,077 to 1,418 mm (LI, 2023). There is a significant spatial gradient, with higher temperatures and lower precipitation in the northwest and lower temperatures and higher precipitation in the southeast. There are distinct wet and dry seasons (Zhang et al., 2006). Alpine meadow is one of the most important grassland types in the SARY, accounting for more than 80% of the total area of the source area, along with alpine grassland and alpine swamp meadow (Zhou et al., 2005; Li et al., 2023), supplemented by alpine early swamps, thickets,





and sparse alpine vegetation (Zhang et al., 2006). However, the area is ecologically vulnerable due to landscape fragmentation caused by the expansion of building land since 1980, coupled with overgrazing, climate change, and vegetation degradation, which accounted for 26.8% of the area in the early 21st century (Zhou et al., 2012). The soil is dominated by alpine meadow and grassland soils with an average thickness of 38 cm, and the carbon and nitrogen reserves are significantly affected by permafrost degradation (Li et al., 2021). As the most important water conservation area in the Yellow River Basin (Mo et al., 2022), the ecological changes in this region play a decisive role in downstream water security. The study showed that the vegetation NDVI showed an improving trend from 2000 to 2019, but the ecological risks caused by permafrost degradation climate warming, and humidification still need to be monitored in the long term (Cao et al., 2021).

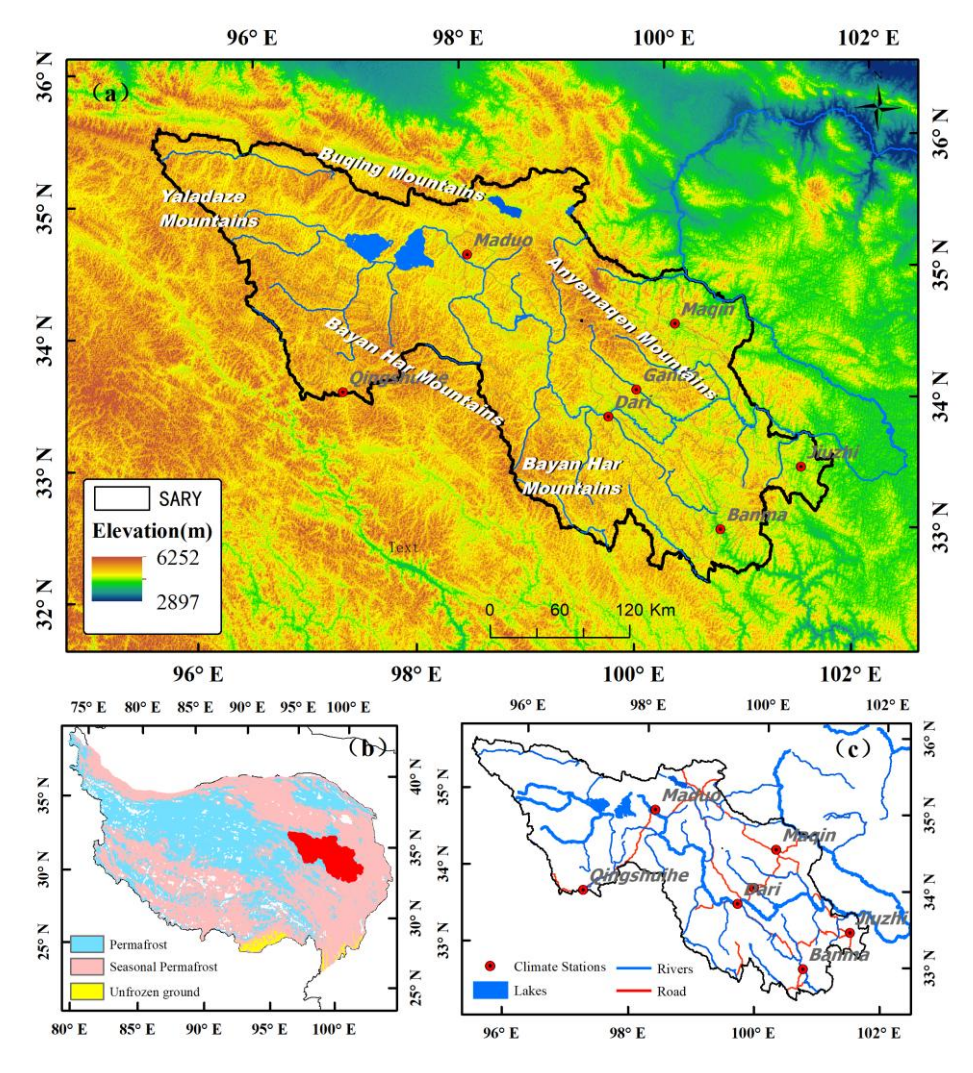


Figure 1. Geographic location of the source area of the Yellow River (SAYR). (a) Background shading indicates a 1-km Digital Elevation Model (DEM) in meters. Red triangles indicate meteorological station locations used in this study; (b)The inset shows the location of SAYR within the Qinghai-Tibetan Plateau;(c) Distribution of meteorological stations, roads, and water systems in the SAYR. Coordinates are in WGS84 (approx. 32.53–35.67°N, 95.11–101.78°E). DEM source: SRTM.





75 **2.2 Datas**

90

2.2.1 Digital Elevation Model (DEM)

In this study, we used the Shuttle Radar Topography Mission (SRTM) digital elevation model (DEM) provided by the United States Geological Survey (USGS). The original resolution of the DEM is 90 m, which was resampled to 1 km to match the spatial resolution of the raster meteorological data. The DEM data were projected to the WGS84 coordinate system and clipped to the extent of the Yellow River source region. The DEM served two major purposes in this study: (i) to provide elevation information as a covariate in the interpolation of meteorological variables, and (ii) to calculate monthly lapse rates used for elevation bias correction of ERA5-Land surface temperature data.

2.2.2 Meteorological Data (CMD and Station Observations)

The meteorological station data and raster data utilized in this study were obtained from the China Meteorological Data Network (http://data.cma.cn). The meteorological raster data (CMD) are monthly datasets with 1 km spatial resolution. They are generated by interpolating long-term station observations using the thin-plate spline method with elevation as an auxiliary variable.

The station data include daily mean air temperature (1.5 m height) and surface temperature (0 cm depth) records from seven meteorological stations in the SAYR for the period 1981–2020. The meteorological station data in this study serve two main purposes: (i) as independent observations for validating both the CMD gridded dataset and the bias-corrected ERA5-Land product, and (ii) they provide the basis for estimating monthly temperature lapse rates, which were subsequently applied to correct elevation bias in ERA5-Land surface temperature fields. All meteorological data underwent rigorous quality control, including value range checks and consistency verification, to ensure the reliability of the datasets.

2.2.3 ERA5-Land Reanalysis Data

The ERA5-Land data, developed by the European Center for Medium-Range Weather Forecasts (ECMWF, https://cds.climate.copernicus.eu), represents the fifth generation of global climate-atmosphere reanalysis data provided by the Copernicus Climate Change Service (C3S) (Muñoz-Sabater et al., 2021). It features a spatial resolution of 0.1° (~10 km), hourly temporal resolution, and improved accuracy compared with its predecessor, ERA-Interim (Frederico Johannsen et al., 2019).

In this study, we selected the ERA5-Land skin temperature (SKT) data for the period 1981–2020. SKT is a physically based variable representing the radiative surface temperature in the surface energy balance. Although ERA5-Land provides high-quality estimates, its relatively coarse resolution may not capture fine-scale topographic variations in mountainous regions such as the SAYR. To address this limitation, we applied an elevation bias correction to ERA5-Land SKT data, using lapse rates derived from station observations in combination with the DEM. Specifically, the monthly lapse rates estimated from CMD and station datasets were used to adjust ERA5-Land SKT to 1 km resolution, thereby improving its representation of





surface temperature variability in complex terrain. This bias-corrected ERA5-Land product was then employed as the primary input for calculating freeze—thaw indices and other surface temperature metrics in subsequent analyses.

2.3 DEM-based surface temperature correction

In mountainous areas with complex topography, the spatial distribution of surface temperatures is strongly influenced by elevation. Traditional horizontal interpolation methods (e.g., Kriging or inverse distance weighting, IDW) only account for horizontal spatial heterogeneity, neglecting the influence of terrain elevation (Chen et al., 2011). This omission can lead to errors of 2–5 °C in high - altitude areas such as the source area of the Yellow River (SAYR), where most elevations exceed 4.000 m.

To improve temperature accuracy, we applied a DEM-based elevation bias correction to the ERA5-Land skin temperature (SKT) product, assuming that elevation is the dominant control of temperature variation. Other factors, such as slope, aspect, or land cover, were not explicitly considered due to data limitations and to preserve model simplicity.

The overall correction procedure consists of three main steps (Figure 2).

Step 1 – Estimation of monthly lapse rates

For each month t during 1981–2020, the monthly mean surface temperature observed at meteorological stations (ST_{obs}) were regressed against station elevation (h) to derive the monthly surface-temperature lapse rate (Γ_t):

$$\Gamma_t = \frac{\sum_i (h_i - \overline{h})(T_i - \overline{T})}{\sum_i (h_i - \overline{h})^2} \tag{1}$$

where, h_i and T_i are the station elevation and observed monthly mean temperature at station i, and \bar{h} and \bar{T} are their means. The corresponding regression relationship can be written as:

$$T_i = a_i + \Gamma_t \cdot h_i + \varepsilon_i \tag{2}$$

where a_i is the intercept, and ε_i is the residual.

 Γ_t (°C/100m⁻¹) is typically negative, reflecting decreasing temperature with increasing altitude.

To ensure the robustness, lapse rate with $|\Gamma_t| > 0.02$ °C m⁻¹ (≈ 2 °C per 100 m), a correlation coefficient $R^2 < 0.2$, or an insufficient number of valid stations ($n < N_{min}$) were replaced by the climatological monthly mean lapse rate (Γ_m) derived from long-term averages.

130 Step 2 – Elevation bias correction and downscaling

The ERA5-Land SKT data (T_0 , 0.1° spatial resolution) was resampled to 1 km by bilinear interpolation, resulting in T_0 1km. The elevation correction was then applied on a pixel-by-pixel basis as:

$$ST = T_{0_{1km}} + \Gamma_t (H_{DEM} - H_{ref}) \tag{3}$$

Where H_{DEM} is the DEM represents the DEM elevation of each 1-km grid cell, and H_{ref} is the mean elevation of the corresponding ERA5-Land grid cell.





This process was implemented in Python (xarray, GDAL, and numpy). The resulting dataset comprises a monthly, 1 km-resolution surface temperature (ST) product for the period 1981–2020.

Step 3 – Accuracy validation

To evaluate the correction, ST was compared with station-based ST_{obs.} Performance metrics include the coefficient of determination (R²), root mean square error (RMSE), unbiased RMSE (ubRMSE), and mean bias error (Bias). Detailed formulas and results are provided in Supplement S1 (Tables S1–S2; Figure S1).

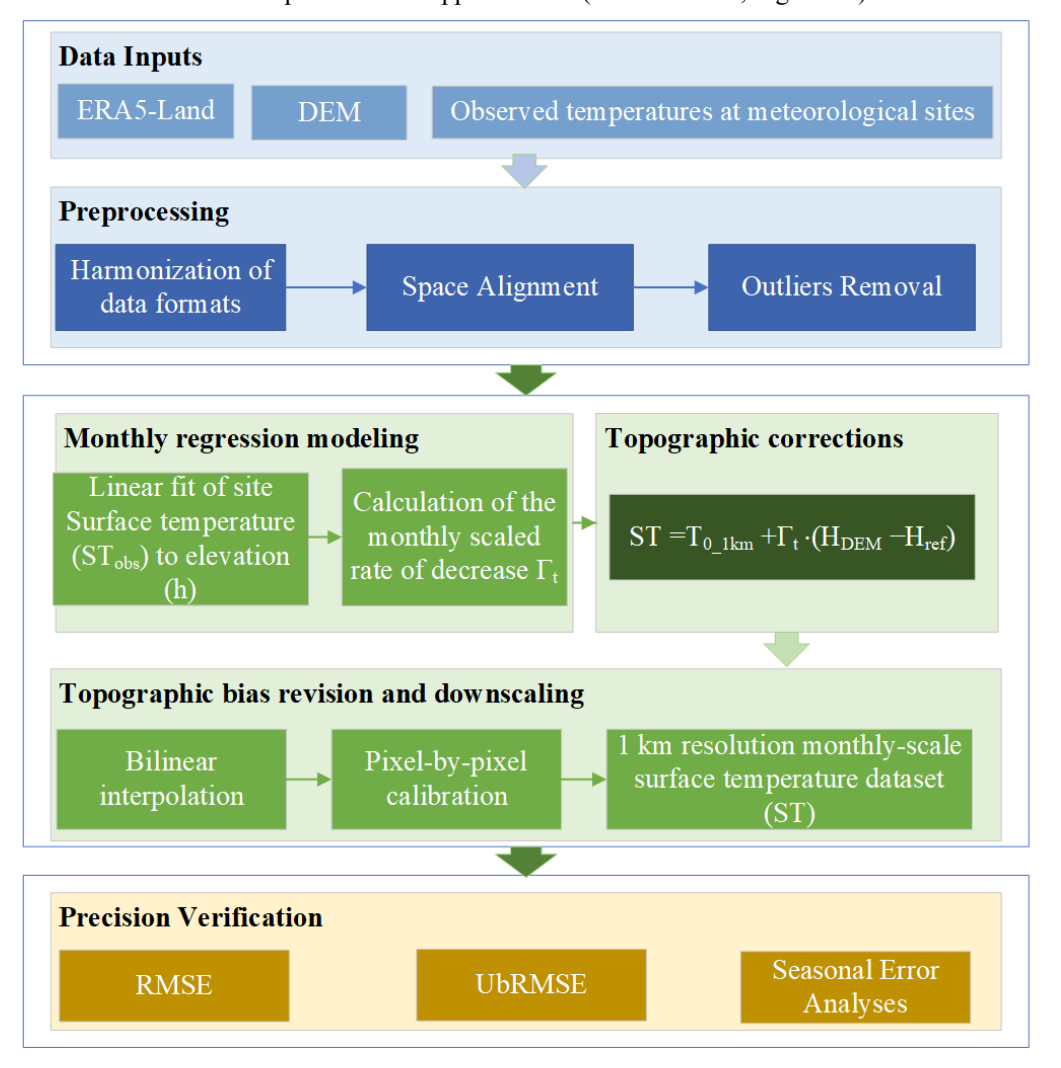


Figure 2. Flowchart of DEM-based elevation bias correction applied to ERA5-Land skin temperature (SKT).





2.4 Freeze-thaw indices and duration of thawing (DOT)

- The freeze-thaw process is a key factor controlling energy and water exchanges in permafrost regions (F. Nelson and S. Outcalt, 1987; Wu et al., 2011; Zheng et al., 2022). To quantitatively characterize freeze-thaw dynamics, both air- and surface-based indices were derived from CMD air temperature and bias-corrected ERA5-Land ST datasets, respectively.
 - Air-based indices (derived from CMD 1 km air temperature): Air Freezing Index (AFI), Air Thawing Index (ATI), and Air Freeze-Thaw Ratio (Na).
- Surface-based indices (derived from DEM-corrected ERA5-Land ST): Surface Freezing Index (SFI), Surface Thawing Index (STI), Surface Freeze-Thaw Ratio (Ng), and Thawing Duration (DOT).

This distinction ensures that atmospheric and surface processes are characterized using their most appropriate data sources.

(1) Definition of freeze-thaw indices:

Following Chen et al. (2021), the freezing and thawing indices (FI, TI) are defined as the cumulative negative and positive temperatures, respectively. Using monthly mean data, they are computed as:

$$FI = \sum_{i=1}^{12} \min(T_t, 0), TI = \sum_{i=1}^{12} \max(T_t, 0)$$
(4)

where T_i denotes the monthly mean temperature, either air temperature ($T_{a,i}$ from CMD) or surface temperature ($T_{s,i}$ from corrected ERA5-Land ST).

The freeze-thaw ratio (N) reflects the relative dominance between thawing and freezing processes and serves as an indicator of permafrost thermal stability (Cheng et al., 2003). It is calculated as:

$$N_a = \frac{ATI}{AFI}, \quad N_g = \frac{STI}{SFI} \tag{5}$$

When N > 1, the thawing process dominates, indicating an increased risk of permafrost degradation; When $N \approx 1$, freezing and thawing are approximately balanced, reflecting relatively stable permafrost conditions; When N < 1, freezing dominates, suggesting stabilization or growth of permafrost at the regional scale.

The monthly thawing index (TI_m) is the sum of positive temperatures for each month, used later for estimating the thawing duration (DOT), while ATI/STI represent annual sums.

Additionally, monthly minimum and maximum surface temperatures (ST_{min} and ST_{max}) were derived from the bias-corrected ERA5-Land surface temperature (ST) dataset. These variables were used to characterize surface temperature extremes and seasonal variability.

170 (2) Thawing duration (DOT)

To quantify the duration of thawing (DOT) in permafrost regions, we established a regression model between the monthly thawing index (TI) and the observed number of thawing days from meteorological stations. This regression was then applied to estimate annual DOT across the SAYR from 1981 to 2020. The regression equation is given as:

$$DOT = \begin{cases} 0.171 \times TI_m + 4.99 , & TI_m \leq 175 \,^{\circ}C \cdot d \\ Dm, & TI_m > 175 \,^{\circ}C \cdot d \end{cases} \tag{6}$$





where a = 0.171 and b = 4.99 are regression coefficients derived from station observations, and Dm denotes the total number of days in the corresponding month (30 or 31). This treatment ensures that months with high TI values are recognized as complete thawing months, while months with smaller TI values are estimated based on regression. Details of the regression validation and the corresponding scatter plot are provided in Supplement Figure S3.

2.5 Mann-Kendall trend test and the Theil-Sen slope estimator

To quantify the long-term trend of the freeze–thaw index, the statistical significance of the time series was assessed using the non-parametric Mann–Kendall test. The trend statistic S was calculated based on the relative size of the data points in the series (see Supplement S3 for the formula). The direction of the trend and the confidence level (α = 0.05 or 0.01) were determined by the standardized test statistic Z_{mk} . If $|Z_{mk}| > 1.96$, the trend is significant at the p < 0.05 level.

The Theil–Sen median method was used to calculate the trend slope β :

185
$$\beta = \text{Median}\left(\frac{x_j - x_i}{j - i}\right) \quad \forall j > i$$
 (8)

Where x_i and x_j are the observed values in years i and j of the time series, respectively. This method is robust to outliers and suitable for analyzing trends in climate data (see Supplement S3 for a detailed derivation).

3 Results and analysis

195

3.1 High-precision surface temperature remote sensing data revision

190 3.1.1 DEM correction of surface temperature data

A linear regression analysis of surface temperature and elevation was conducted using monthly mean surface temperature data from seven meteorological stations in the SAYR. The findings indicated that the use of DEM-corrected surface temperature exhibited a superior ability to align with the monthly mean surface temperature of the stations within the study area. Additionally, the coefficients of determination (R^2) values were all greater than 0.5, signifying the significance of the elevation factor in shaping the surface temperature distribution within the study region. The person's correlation coefficient was subsequently employed to calculate the vertical lapse rate (Γ) of the mean surface temperature in the study area, yielding a result of 0.63 °C/100 m. Furthermore, given the substantial discrepancy in surface temperature between the warm and cold seasons in the SAYR, this study endeavored to characterize its temporal and spatial changes with greater precision. To this end, the vertical lapse rate of surface temperature was estimated every month (Table S1).

An analysis of the vertical lapse rate data in December reveals that the Yellow River source region exhibits the most pronounced lapse rate during winter (-0.85 °C/100m, R²=0.952) and the least significant lapse rate during summer (-0.43 °C/100m, R²=0.852). This phenomenon can be attributed to the pronounced radiative cooling experienced at the surface during winter months, coupled with the enhanced heat dissipation observed in the high-altitude region. This dynamic leads to an increase in the temperature gradient. Concurrently, the stable snow accumulation in the SAYR during winter, in conjunction





with the high surface albedo, contributed to the exacerbation of the temperature drop in the high-altitude zone, particularly in January, the coldest month. The model with a vertical decrement rate of -0.90 °C/100m exhibited the strongest explanatory power, as indicated in Table S1 and Figure 3. On this basis, the ERA5-Land skin temperature product (SKT) was revised in conjunction with the Digital Elevation Model (DEM). The result was a month-by-month time-series surface temperature dataset (ST) with a 1 km resolution for the period 1981-2020, totaling 40 years of time-series data.

210 **3.1.2 Validation**

215

220

225

In this study, a correlation analysis was conducted between the ST_{obs} and the corrected ST dataset. The results demonstrated a high correlation between ST and ST_{obs}, with an R² value of 0.939 (Figure 4). This finding indicates that the dataset can effectively reflect the spatial and temporal distribution of ST in the SAYR. A certain degree of overestimation is observed during the cold season, which may be attributable to the systematic bias of the ERA5-Land SKT data under low-temperature conditions. For the growing season, the site-scale root mean square error (RMSE) was 1.22 °C, and the unbiased root mean square error (ubRMSE) was 0.38 °C. These values suggest that the ST dataset is highly accurate during the growing season in the SAYR. Additionally, the monthly mean RMSE and ubRMSE for the ST dataset were 1.90 °C and 1.21 °C, respectively. The ST root mean square error (RMSE) and unbiased root mean square error (ubRMSE) in winter were reduced by 81 % and 36%, respectively, which significantly improved the accuracy of temperature estimation in alpine regions(Table S2 and Figure S1). The DEM-corrected 1 km resolution ST data demonstrate a more reasonable spatial distribution pattern in comparison with ST_{obs}. This is due to the former's ability to more accurately portray the details of the temperature field in mountainous areas.

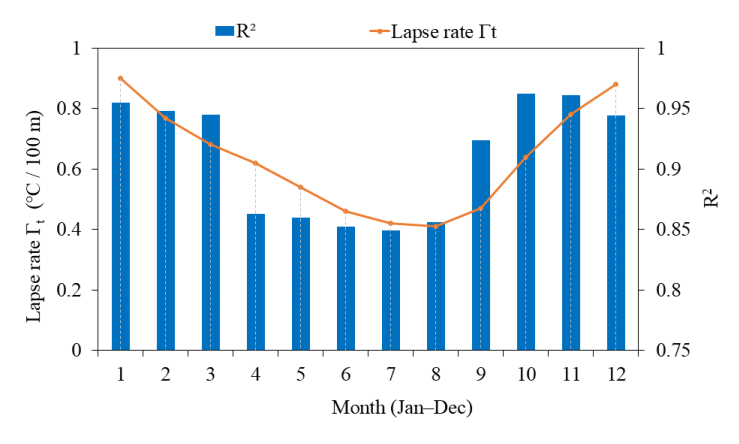


Figure 3. Monthly variation of the surface temperature lapse rate Γ (°C /100 m) estimated from station observations in the SAYR. Error bars = ± 1 standard deviation of monthly site estimates. Winter months show the largest absolute lapse rates (e.g. Dec: -0.85 °C/100 m, R^2 =0.952).





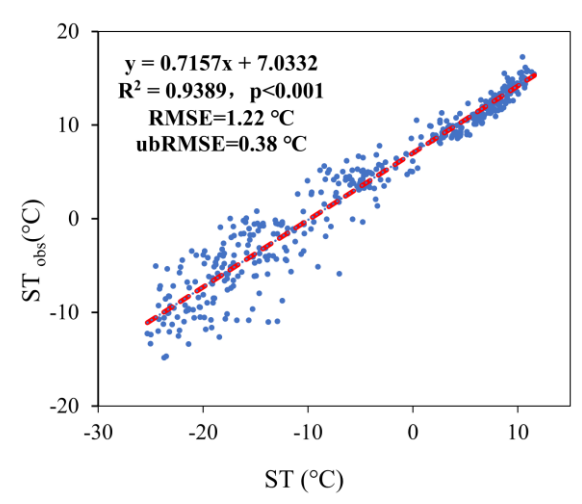


Figure 4. Scatterplot of DEM-corrected monthly surface temperature (ST, °C) versus station observations (ST_{obs}, °C). Each point = monthly mean; dashed line = linear fit ($R^2 = 0.939$). RMSE (growing season) = 1.22 °C, ubRMSE = 0.38 °C. Cold-season overestimation is noted (see text).

3.2 Characterization of temporal and spatial variations in the freeze-thaw cycle

3.2.1 ST changes in the SAYR

230

235

240

During 1981–2020, the surface temperature (ST) in the SAYR exhibited a significant upward trend. The multi-year mean ST was 3.54 °C, with an overall warming rate of 0.31 ± 0.02 °C/10a(Figure 5). Before 2000, the annual mean ST increased at a modest rate of 0.10 °C/10a, while after 2000 the rate accelerated to 0.25 °C/10a, about 2.5 times higher. This shift indicates an enhanced sensitivity of permafrost in the SAYR to recent climate warming.

The trends of extreme temperature indices further highlight seasonal differences. The daily maximum ST (ST_{max}) decreased slightly at -0.19 °C/10a, while the daily minimum ST (ST_{min}) increased strongly at 1.4 °C/10a. Consequently, the diurnal ST range narrowed significantly at -1.61 °C/10a, suggesting that winter warming exceeded summer warming. This asymmetric warming indicates that permafrost in the SAYR is particularly vulnerable, as the reduction in winter cooling limits frost penetration and accelerates active-layer deepening. Overall, the combined trends of rising mean ST, increasing ST_{min} , and narrowing diurnal surface temperature range all point to enhanced permafrost degradation risks in the SAYR.





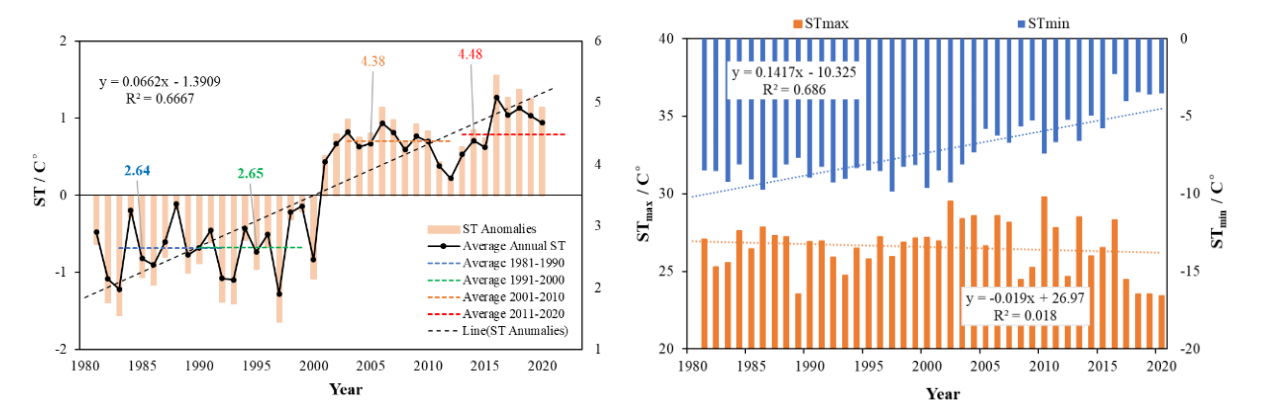


Figure 5. Interannual variations of mean surface temperature (ST), daily maximum (ST_{max}), daily minimum (ST_{min}), and diurnal surface temperature range in the Source Area of the Yellow River (1981–2020). Linear trends are shown with corresponding decadal rates.

3.2.2 Spatial distribution of freeze-thaw indices

The spatial distribution characteristics of the Atmospheric Freeze Index (AFI) and Surface Freeze Index (SFI) in the SAYR demonstrate a discernible spatial correlation with altitude. Specifically, both AFI and SFI demonstrate a distribution trend of high in the west and low in the east, with a concurrent decrease from the northwest to the southeast (Figure 6a, c). The AFI decreases from a westernmost range of 9385.07 °C·d to an easternmost range of 297.7 °C·d, with a regional mean of 2274.25 °C·d. Meanwhile, the SFI decreases from 3119.73 °C·d in the westernmost range to less than 50 °C·d in the easternmost range, with a regional mean of 900.01 °C. The highest values of both are in the Marduo area, and the lowest values are in the Banma area. The SFI exhibits greater spatial variability than the AFI, suggesting that surface temperature is more strongly influenced by topography. This distributional feature aligns with the findings of Wang et al. (2019a).





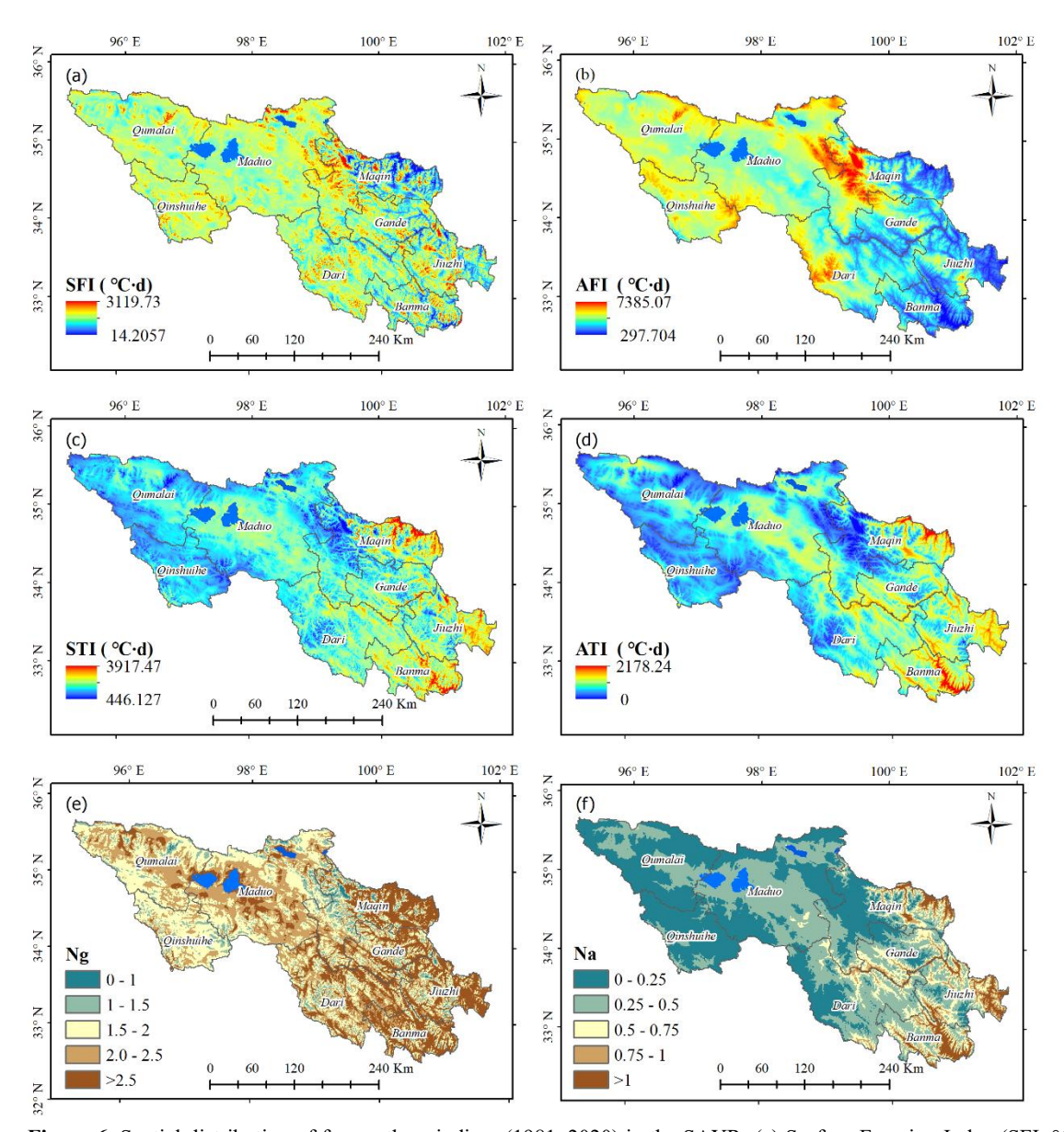


Figure 6. Spatial distribution of freeze-thaw indices (1981–2020) in the SAYR: (a) Surface Freezing Index (SFI, °C·d); (b) Air Freezing Index (AFI, °C·d); (c) Surface Thawing Index (STI, °C·d); (d) Air Thawing Index (ATI, °C·d); (e) Surface freeze-thaw ratio (Ng, unitless); (f) Air freeze-thaw ratio (Na, unitless). All indices are computed from 1 km grids (SFI/STI from DEM-corrected ST; AFI/ATI from CMD air temperature). Colorbars show index values; higher SFI/AFI indicate stronger freezing.

In contrast to the freezing index, the Atmospheric Thawing Index (ATI) and Surface Thawing Index (STI) exhibited a spatial distribution indicative of low west and high east, with a decrease from southeast to northwest Figure 6b,d). The range of the ATI was found to be from 681.53 to 2178.24 °C·d, with a mean value of 681.53 °C·d. The STI ranged from 446.13.24 to 3917.47 °C·d, with a mean value of 1896.35 °C·d. The highest values of both variables are observed in the Baima area, while



275

280

285



the lowest values are recorded in the Maqin area. Furthermore, the amplitude of spatial variability of STI is greater than that of ATI, suggesting that the warming effect of the land surface is more pronounced.

The air thaw ratio (Na) ranges from 0.44 to 2.85, with a mean value of 1.24, indicating a distribution of low in the west and high in the east, with Na < 1 in Maduo, Gande, and Dari (Table 1). This finding suggests that freezing capacity remains predominant. In Jiuzhi and Banma, Na >1 suggests an escalation in the degradation of perennial permafrost. The ground thaw ratio (Ng) ranges from 1.31 to 5.73, with a mean value of 2.73. The ground thaw ratios are typically greater than 1, and their distribution demonstrates a tendency to increase with decreasing altitude from west to east (Figure 6e. The Maduo, Gande, and Dari regions, with a freezing capacity index (Ng) of less than 2, continue to be dominated by freezing capacity. In contrast, the Banma region, with a freezing capacity index (Ng) greater than 5, exhibits a significant increase in thawing capacity. The trend of permafrost degradation is the most evident in this region (Table 1). As the melting index increases and the freezing index decreases, the thaw-to-freeze ratio increases significantly, indicating that the degradation of perennial permafrost is accelerating.

As demonstrated in Table 1, the magnitude of change in the temperature freeze—thaw index and the magnitude of change in the surface freeze—thaw index exhibited significant variation across different altitudes, temperatures, and surface coverages. Notably, the magnitude of change in the surface freeze—thaw index surpassed that of the atmospheric freeze—thaw index. Concurrently, the annual mean air temperature at each site is considerably lower than the surface temperature, and the heating effect of the surface on the atmosphere is greater than the cooling effect. The magnitude of Ng is considerably higher than Na at each site, suggesting that the surface temperature is elevated relative to the air temperature during the warm season. However, the magnitude of Ng has been substantially diminished with the rise in air temperature, indicating that the perennial permafrost is undergoing a thawing trend. Although the value of Ng >1 at all sites in the SAYR, the thaw-to-freeze ratio exhibits a significant increase.

Table 1. Freeze-thaw indices and n-factors for air and ground temperatures

Site	DEM	AT	ST	ATI	AFI	Na	STI	SFI	Ng
Maduo	4273.1	-3.12	1.46	877.97	1977.71	0.44	1817.24	1384.23	1.31
Maqin	3719.8	0.22	4.29	1353.32	1243.50	1.09	2306.02	902.44	2.56
Gande	4050.8	-2.08	1.76	1018.89	1742.48	0.58	1878.06	1292.78	1.45
Dari	3968.3	-0.29	2.85	1246.49	1327.13	0.94	2027.98	1006.59	2.01
Jiyzhi	3629.3	1.30	4.57	1461.79	958.50	1.53	2241.12	675.07	3.32
Banma	3530.8	3.23	6.49	1851.42	649.47	2.85	2850.48	497.74	5.73



295

300

305



3.2.3 Temporal and spatial trends in Freezing Index

From 1981 to 2020, both the AFI and SFI in the SAYR showed significant interannual decreasing trends (Figure 7a,b), decreasing at rates of -100.43 °C·d/10a and -141.85 °C·d/10a, respectively. Before 2000, the decreasing rate of SFI (5.64 °C·d/10a) was significantly lower than that of the AFI (88.52 °C·d/10a). After 2000, the decrease in the freezing index accelerated, particularly the decrease in SFI, which decreased to 207.24 °C·d/10a from 2001 to 2010 and decreased further to 721.77 °C·d from 2010 to 2020. Over the past 40 years, AFI decreased by 286.9 °C·d and SFI decreased by 389.72 °C·d. This trend is consistent with that of ST_{min}, indicating that the stability of perennial permafrost continues to weaken.

With respect to spatial changes (Figure 7), the AFI exhibited a downward trend across all regions, with the exception of a slight uptick in the northeastern Maqin region. The rate of decline increased in a northerly to southerly direction, and SFI demonstrated a slight increase in the northwestern Qumalai and southeastern Baima regions. Concurrently, SFI underwent a decrease to varying extents in the remaining regions. Notably, the northeastern Maqin region experienced the most substantial decline, with a drop exceeding 150 °C/10a. Overall, in the last 40 years, the stability of perennial permafrost has continued to weaken. The decline in FFI observed in the SAYR over the past four decades is of particular significance, suggesting that the permafrost is undergoing rapid degradation.

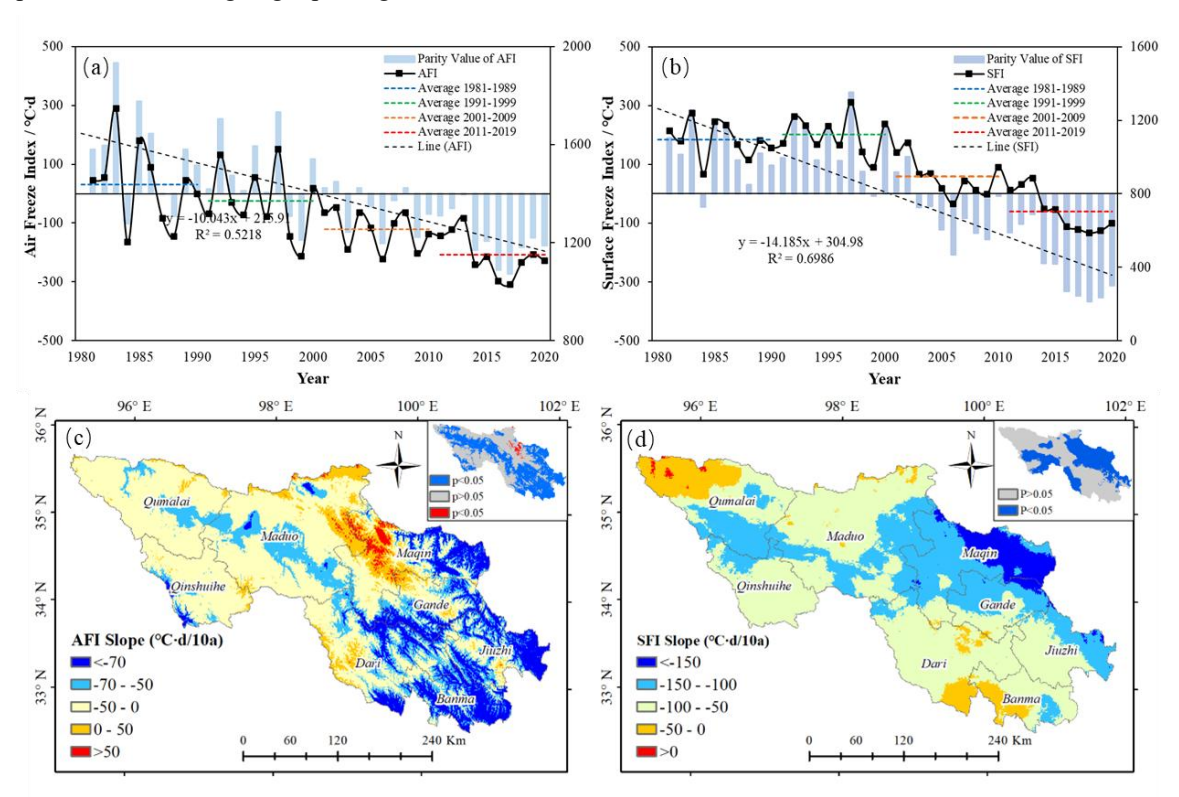


Figure 7. Interannual trends of freezing indices (1981–2020). (a-b) Time series of region-mean AFI and SFI with linear lines (p<0.05); (c-d) Spatial distribution of trend slopes (Theil–Sen estimate, units °C·d/10a) and significance (Mann–Kendall). Positive slopes indicate warming/thawing trends; negative slopes indicate cooling/freezing trends.

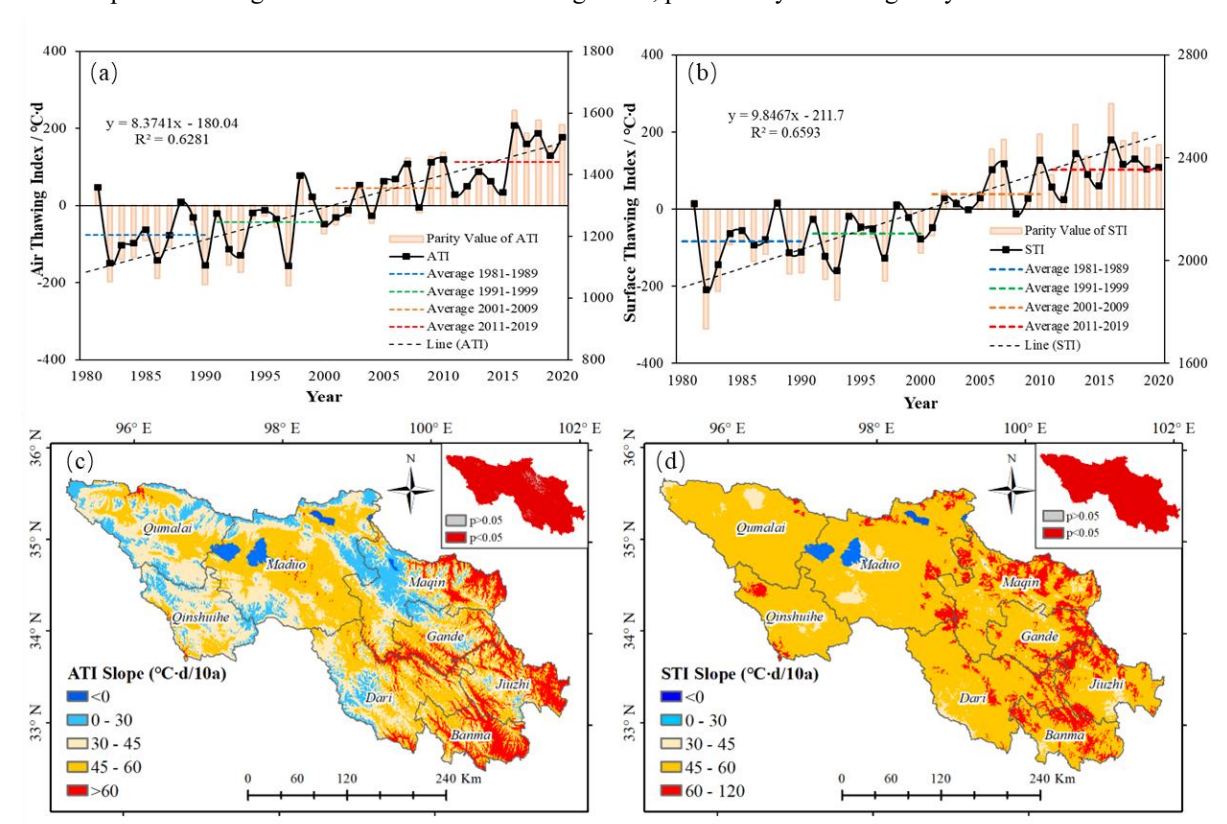


320



3.2.4 Temporal and spatial trends in the Thawing Index

SAYR exhibited a substantial increase in both ATI and STI, with a p-value of less than 0.001, on an interannual scale from 1981 to 2020. The growth rates recorded were 83.74 °C·d/10a and 98.47 °C·d/10a, respectively, as depicted in Figure 8a, b. Before the year 2000, the growth rates of ATI and STI exhibited a gradual rise, reaching 38.25 °C·d/10a and 34.17 °C·d/10a, respectively. However, since the year 2000, there has been a substantial increase in the growth rate of ATI, reaching 112.47 °C·d/10a. Similarly, the growth rate of STI has also shown a notable rise, reaching 105.01 °C·d/10a, which is approximately three times the growth rate observed before the year 2000. Concurrently, the rate of change of both ATI and STI has proven to be greater than that of the freezing index, particularly following the year 2000.



315 **Figure 8.** Interannual trends of thawing indices (1981–2020). (a-b) Time series of region-mean ATI and STI with linear lines (p<0.05); (c-d) Spatial distribution of trend slopes (Theil–Sen estimate, units °C·d/10a) and significance (Mann–Kendall). Positive slopes indicate warming/thawing trends; negative slopes indicate cooling/freezing trends.

The accelerated rise in air and ground temperatures during the thawing period, in conjunction with the freeze-thaw cycle, is increasingly dominated by the thawing process. The spatial distribution trend (Figure 8c, d) exhibited a contrasting pattern to the freezing index distribution trend. The rate of increase in ATI in the majority of the SAYR gradually increased from southeast to northwest, with the most significant increases observed in the areas of Maqin, Jiuzhi, and Bama, among others.





The STI demonstrated a marked increase in the entire Yellow River source region (p < 0.05), with the rate of increase exceeding $30^{\circ}\text{C}\cdot\text{d}/10a$.

3.2.3 Temporal and spatial trends in duration of thawning

Based on the DOT model described in Section 2.4, which was established from the regression relationship between monthly thawing index (TI) and thawing days using meteorological station observations, we estimated the regional thawing duration (DOT) using the DEM-corrected ERA5-Land ST dataset for 1981–2020. According to the results (Figure 9), the regional mean DOT exhibited an overall increasing trend of 6.61 d/10a over the past 40 years, with a multi-year average of 229.05 d. Before 2000, the variability of DOT was minimal, decreasing slightly from an average of 222.37 d in the 1980s to 223.48 d in the 1990s. It then increased to 228.9 d in the 2000s and further to 241.4 d in the 2010s.

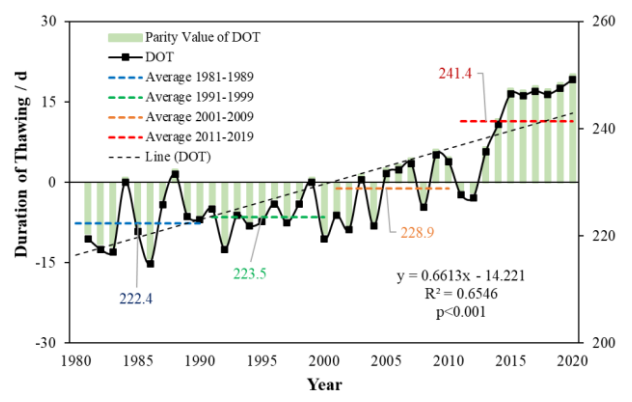


Figure 9. Interannual trends (1981–2020) of the regionally averaged duration of thawing (DOT, days). Linear trend lines are shown, with statistically significant trends (p < 0.05).

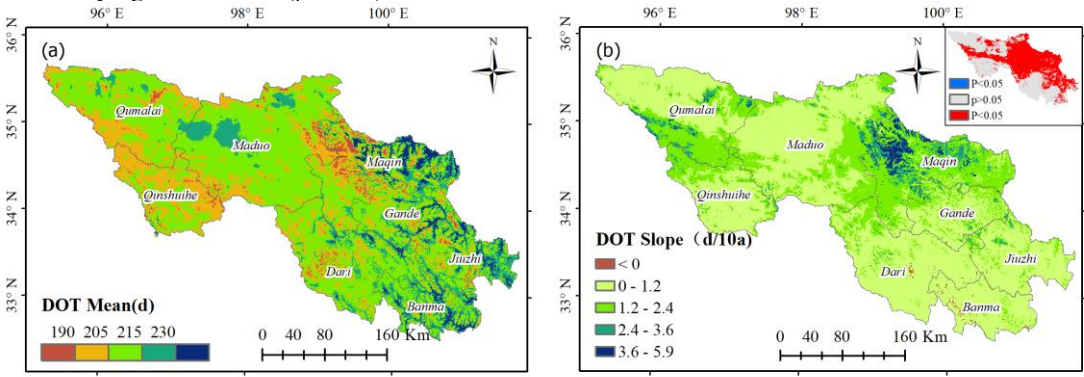


Figure 10. Spatial distribution of thawing duration (DOT, days) averaged over 1981–2020 (a) and its spatial trend (Theil–Sen slope, days per decade; b). Trend significance (Mann–Kendall, p < 0.05) is hatched.

As illustrated in Figure 10, the spatial distribution of DOT ranged from 95 to 319 days, with a clear gradient of short duration in the northwest and long duration in the southeast. In the low-altitude southeast zone, thawing typically began in early April and lasted until late October, exceeding 230 days in duration. By contrast, in the high-altitude region of the northwest, such as





the Mado area and the Qingshui River basin, DOT was less than 180 days. Over the past four decades, the mean DOT across the entire region exhibited an increase of 1.17 d/10a, with the southeastern low-elevation zone showing the strongest extension (3.6 d/10a). This phenomenon may be linked to the enhanced thermal insulation effect from increased vegetative cover. Overall, the significant prolongation of DOT in the SAYR confirms the ongoing degradation of perennial permafrost.

4 Discussions

345

350

355

360

365

370

4.1 Data applicability

In the context of climate change research, the necessity of extensive, long-term climate data series, often spanning a century or more, is paramount. However, the Tibetan Plateau region presents a unique challenge in this regard due to the limited observation history, sparse distribution, and heterogeneous nature of meteorological stations. This poses a significant obstacle in studying perennial permafrost changes based solely on measured data. Consequently, extant studies frequently employ reanalyzed datasets (e.g., ERA, CRU, MERRA2) to evaluate the climate and environmental evolution of the region. Nevertheless, the existing reanalysis data continue to exhibit substantial limitations in the context of permafrost change research. On the one hand, the CRU month-by-month temperatures offer monthly-scale cardinal details, which may lead to some bias in the calculation of freeze-thaw indices compared to the daily average temperatures, especially during periods of alternating freezing and thawing (e.g., early summer and fall/winter seasons). This may result in an underestimation of the persistence of the freezing process or an overestimation of the energy accumulation during the thawing period due to the lack of high temporal resolution data. Conversely, the spatial resolution of the ERA5-land data is 0.1° (approximately 1500 km²/grid point), and the elevation change at this scale can be hundreds or even thousands of meters in the Tibetan Plateau, where the topography is highly complex. When the Lapse Rate Effect is taken into consideration, it becomes evident that the freezing and thawing indices calculated directly from ERA5-Land SKT data are likely to be subject to overestimation or underestimation. To illustrate, the raw ERA5-Land data have the potential to overestimate surface temperature and underestimate the freezing index at elevated altitudes, while the reverse trend may be observed at lower altitudes. In order to enhance the applicability of ERA5-Land data in the SAYR, this study systematically evaluated the impact of complex topography and local factors. The study implemented a high-resolution downscaling process for ERA5-Land SKT data through DEM correction and data validation at meteorological stations. The SAYR exhibits a wide distribution of high and low rolling hills, and the substantial altitude difference results in significant vertical changes in climate. The ST is low. The mean vertical lapse rate of ST in the SAYR was 0.63 °C/(100 m), with significant seasonal variations. The maximum vertical lapse rate was observed in December (0.9 °C/(100 m)), while the minimum was recorded in August (0.41 °C/(100 m)). This result aligns closely with the findings of Chen et al. (2025) in the Qinghai-Tibetan Plateau, where the vertical lapse rate of ST in July was 0.47 °C/(100 m), and with those of Lin et al. (2018) in the Qilian Mountains, where the average vertical lapse rate of ST was 0.60 °C/(100 m), reaching a maximum of 0.91 °C/(100 m) in December. In consideration of the vertical lapse rate of surface temperature in various altitude regions, the DEM-based spatial interpolation method is employed to revise



380

385

400



the surface temperature every month. This approach effectively corrects the ERA5-Land data, thereby ensuring greater consistency with the characteristics of the actual terrain distribution. When combined with ST_{obs} for error assessment and optimization, the surface temperature estimation error caused by topographic complexity was significantly reduced. As a result, a high-precision ST dataset was generated with a resolution of 1 km. This dataset provides more reliable temperature-driven data for the study of the spatial and temporal evolution of the freeze—thaw cycle.

Despite the efficacy of the DEM-based correction in enhancing the spatial accuracy of the ERA5-Land SKT data, residual uncertainties persist. On the one hand, given that the initial resolution of ERA5-Land is 0.1° (approximately 10 km), the issue of inadequate elevation response may persist even after correction within the intricate topography of the Yellow River source region. Conversely, the number of meteorological stations is restricted to only seven, with the majority situated within the convenient transportation area. This limitation results in a constrained spatial representation. Consequently, future research endeavors may enhance spatial integrity and accuracy by integrating multi-source remote sensing products.

4.2 Elevation gradient effects and ecohydrological impacts of freeze-thaw indices

The atmospheric freezing and thawing index are primarily governed by large-scale environmental conditions, including air temperature, solar radiation, air humidity, and atmospheric circulation. Meanwhile, the spatial differentiation of the surface thermal state and the freeze—thaw process is strongly influenced by elevation as well as local surface properties such as vegetation cover, soil moisture, and thermal conductivity. At the macro scale, latitude, longitude, and especially elevation exert a dominant control on freeze—thaw variability, while at the micro scale, factors such as slope aspect, vegetation density, and soil moisture modulate local conditions.

In the SARY, the spatial distribution of freeze-thaw indices exhibited a pronounced elevation gradient effect. Specifically, freezing indices (AFI, SFI) decrease with declining elevation, while thawing indices (ATI, STI) increase, reflecting stronger freezing in the high-altitude zones and enhanced thawing in lower-altitude valleys (see Figure S3 in the Supplement). The correlation between elevation and thawing indices ($R^2 = 0.63$, p < 0.001) is notably stronger than that with freezing indices, underscoring the dominant role of elevation in controlling freeze-thaw dynamics.

395 The SAYR lies between the BaYan Kala Mountains and the Animachin Mountains. The windward slopes, cold and humid air masses contribute to higher freezing indices, whereas valley regions experience higher thawing indices due to subsidence warming. This pattern is consistent with that of Gao et al. (2023), emphasized the role of elevation in shaping permafrost distribution via temperature gradients and surface energy balance.

Furthermore, our results also reveal that regions' surface thaw indices below 1600 °C·d are concentrated in high-elevation zones (above 4600 m), such as Zorlaiza, Bayan Kara Pass, and Zhuoya Daze. In these alpine wetlands, dense vegetation and high soil moisture increase surface albedo and soil heat capacity, thereby reducing heat input and lowering thawing indices. This finding agrees with Li et al. (2020), who demonstrated that alpine meadows vegetation substantially modulates solar radiation and enhances the thermal stability of permafrost.



410

415

430

435



Thus, the combined influence of elevation, vegetation, and soil moisture drives the spatial pattern of freeze—thaw indices, highlighting the ecohydrological significance of elevation-related processes in permafrost regions.

4.3 Trends in perennial permafrost degradation and its ecohydrological implications

The TI in the SAYR is found to be considerably higher than the TI, suggesting that the freeze–thaw cycle in this region is predominantly governed by the thawing process. This indicates that the perennial permafrost is experiencing an accelerated degradation trend. The surface thaw-thaw ratio (Ng) exhibited a higher value in comparison to the air thaw-thaw ratio (Na), demonstrating an increase that propagated from the northwest to the southeast (Ng > 2.0 was prevalent in the southeast). This observation signifies that the surface thaw depth persisted in its increase, concurrent with a gradual deepening of the active layer, a phenomenon that occurred in conjunction with the accumulation of heat within the permafrost. This phenomenon aligns with the findings of Zhang et al. (2024), employing the TTOP model, predicted multi-year permafrost degradation. A general consensus emerges from the available data regarding the increasing multi-surface temperature (ST) in the SAYR. This phenomenon is concomitant with the decreasing trend of the freezing index and increasing trend of the thawing index (see Figure 7-8). This observation indicates a decline in the stability of the perennial permafrost. In particular, in areas with lower elevations and substantial vegetation cover, the thawing period persisted, with a duration exceeding 230 days. This prolonged thawing resulted in a significant accumulation of permafrost heat.

The joint evolution of these indicators clearly reflects the degradation trend of perennial permafrost in the SAYR. The continuous degradation of perennial permafrost may have far-reaching impacts on ecosystems and hydrological processes. Permafrost thawing has been shown to increase soil water availability and promote vegetation growth. However, this phenomenon may also exacerbate soil carbon emissions and affect the regional carbon cycle (Peng et al., 2019). The thickening of the active layer has been shown to enhance subsurface microbial activities and accelerate soil organic matter decomposition, resulting in the release of greenhouse gases (Li et al., 2024). Conversely, multi-year permafrost has been shown to lead to increased groundwater runoff, thereby altering the hydrological cycle pattern and affecting the runoff process in the upper reaches of the Yellow River. The extension of the summer thaw period may result in an increase in the seasonal net flow in the SAYR. Conversely, the reduction of the winter freeze period may intensify the seasonal water shortage problem.

The SAYR is located at the intersection of perennial permafrost and seasonal permafrost, and the surface thaw time is mainly controlled by elevation, which shows a significant spatial gradient, with longer thaw time in the southeastern low-elevation zone and shorter thaw time in the northwestern high-elevation zone. This is consistent with the findings of Gao et al. (2023) and Wang (2019a) that the higher the altitude, the lower the atmospheric pressure, the thinner the space, the weaker the insulation effect, the slower the temperature rise at higher altitudes, the longer the time the ground is in a frozen state, and the shorter the thawing period. The lower the altitude, the faster the temperature rises, combined with the increased thermal insulation of vegetation in the southeast of the source area, prolongs the melting period. Meanwhile, the observed increase in thaw duration (1.2 d/10a) in the SAYR is consistent with the pan-Arctic trend of permafrost degradation (Biskaborn et al.,



440



2019; Obu et al., 2019), suggesting a synchronous response of permafrost to anthropogenic forcing at both mid- and high latitudes. This is closely linked to temperature increases and changes in the surface heat balance associated with global warming, leading to shorter surface freezing periods and earlier and longer thawing periods, which in turn affect regional hydrological processes and ecosystem stability. In addition, permafrost degradation poses a potential threat to the safety of regional infrastructure. For example, in areas of road and dam construction, the increased thickness of the active layer can lead to a reduction in the bearing capacity of the foundations, which can induce engineering diseases such as pavement cracking and pipeline fracture (Hjort et al., 2022; Ran et al., 2022). Therefore, the results of this study are an important reference for future infrastructure site planning and design.

4.4 Vegetation's role in regulating the freeze-thaw cycle

445 Vegetation has been identified as a critical factor influencing the thermal stability of permafrost, which exerts a substantial effect on the freeze-thaw cycle index and the duration of the thaw period by modifying the surface energy balance, regulating soil moisture, and influencing albedo and transpiration (Gao et al., 2023). The spatial differentiation of the freeze-thaw index in the Yellow River catchment is influenced by climatic factors as well as the type and cover of surface vegetation. As demonstrated in Figure 8, the STI exhibited a marked increase in the alpine meadow and wetland vegetation area in the 450 southeast relative to the grassland bare rock area in the northwest. This phenomenon is closely related to the thermal insulation effect of high vegetation cover. As demonstrated in related studies (Shen et al., 2015; Li et al., 2020), alpine meadows have been shown to slow permafrost degradation by increasing the surface soil heat capacity and reducing the magnitude of daily changes in soil temperature. During summer months, the process of transpiration in alpine meadows has been observed to reduce soil temperatures by 0.5-1.2°C (Shen et al., 2015). This phenomenon functions as a cooling agent, thereby indirectly inhibiting the growth of the thaw index. During the winter months, vegetation plays a pivotal role in regulating surface heat 455 dissipation, functioning as a form of thermal insulation, and thereby reducing the freezing index (Li et al., 2024). Areas exhibiting elevated surface vegetation cover (e.g., the southeast) demonstrated higher thaw/freeze ratios (Ng > 2.0), indicating that as vegetation succession progresses in response to climate warming, meadow areas may experience an augmentation in surface heat accumulation, an extension of thaw periods, and acceleration in the degradation of perennial permafrost.

In this study, the effect of local microtopography (e.g., valley winds) on surface temperature was not taken into account, which may lead to a bias in the calculation of local freezing and thawing indices. The spatial interpolation accuracy can be further improved in the future by combining higher-resolution DEM and remote sensing data (Sentinel-3 LST). In addition, the missing SKT data (<5%) due to cloud cover were filled by linear interpolation in this study, which may affect the temperature accuracy in some areas. In the future, data fusion can be performed by combining multi-source remote sensing data, such as MODIS LST and Sentinel-3 LST, to improve data completeness and reliability.





5 Conclusion

470

475

480

485

In this study, we developed a 1 km freeze-thaw dataset of the SAYR from 1981 to 2020. This dataset was constructed using DEM-corrected ERA5 land SKT data. The construction of this dataset solved the difficult problem of temperature downscaling in high-elevation and complex terrain areas. It also significantly improved the accuracy of ST estimation (RMSE=1.22 °C, ubRMSE=0.38 °C). The findings indicate a substantial decline in the air and surface freezing indices within the source region of the Yellow River over the past four decades. This decline is evident in the observed decrease of -100.43 °C/10a and -141, respectively. As the temperature increased from 85°C to 100°C, the thawing indices exhibited a consistent upward trend, reaching 83.74°C/10°C and 98.47°C/10°C, respectively. Furthermore, the thawing ratio, N, consistently exceeded the value of 1 and demonstrated an upward trajectory, suggesting a discernible trend of multi-year permafrost degradation. Concurrently, the duration of thaw (DOT) exhibited a marked increase at a rate of 1.2 d/10a, particularly in the southeastern region characterized by lower elevations, which proved to be the most substantial. The freeze-thaw cycle in the SAYR exhibits a discernible topographic gradient distribution, which is collectively governed by elevation, climate warming, and vegetation type. The freezing capacity remains robust in the high-altitude region, while the thawing process is accelerated in the lowaltitude area. These observations suggest that topography and ecological factors play a pivotal role in determining the stability of permafrost. The accelerated degradation of permafrost has far-reaching consequences for alpine ecosystems, including alterations to water cycling, vegetation succession, and carbon flux. This phenomenon also poses a significant challenge to infrastructure security. The consolidation of the thaw layer may result in a reduction of foundation stability, thereby increasing the likelihood of roadbed impairment thawing and subsidence. Consequently, the findings of this study offer a scientific foundation for the establishment of ecological protection red lines, the development of climate-adapted infrastructure planning, and the assessment of regional permafrost risk. The findings of this study indicate that permafrost may incur heightened degradation risks in the context of future climate warming, suggesting that permafrost may be susceptible to more severe degradation risks in the future.

Data Availability Statement

A dataset of monthly land surface temperature at a resolution of 1 km (based on DEM-corrected ERA-Land) and annual free ze-thaw indices (1981–2020) in SAYR is available from the Figshare repository (Li et al., 2025a, 2025b). DEM-corrected te mperature (https://doi.org/10.6084/m9.figshare.29261540) and freeze-thaw indices (https://doi.org/10.6084/m9.figshare.29261555). All the data are provided as GeoTIFF files (.tif). The other datasets used in this study are publicly available via the websites referenced in the paper. (LI et al., 2025a, 2025b)

495 Author contributions

HL and FL conceived the idea. HL developed the methodology, handled the coding, and wrote the original draft. FL and QZ provided guidance on the methodology and reviewed and edited the manuscript. YC helped refine the work. YC, SW, YY, and CC collected and processed the data. All authors contributed to the writing.





500 Competing interests

The contact author has declared that none of the authors has any competing interests.

Disclaimer

Publisher's note: Copernicus Publications remains neutral with regard to jurisdictional claims made in the text, published maps, institutional affiliations, or any other geographical representation in this paper. While Copernicus Publications makes every effort to include appropriate place names, the final responsibility lies with the authors.

Acknowledgements

We thank the China Meteorological Data Service Centre (CMDC) for providing meteorological data, the European Center for Medium-Range Weather Forecasts (ECMWF) for providing ERA5-Land data products.

Financial support

This research was funded by the Qinghai Institute of Technology "Kunlun Yingcai" talent introduction of scientific research projects (grant no. 2023-QLGKLYCZX-023), the Key Fund of the National Natural Science Foundation of China (grant no U2240204), and the National Key R&D Program of China (grant no. 2019YFA0606902)

References

515

- A. Klene, F. Nelson, N. Shiklomanov, and K. Hinkel: The N-factor in Natural Landscapes: Variability of Air and Soil-Surface Temperatures, Kuparuk River Basin, Alaska, U.S.A, Arctic, Antarctic, and Alpine Research, https://doi.org/10.1080/15230430.2001.12003416, 2001.
- Biskaborn, B. K., Smith, S. L., Noetzli, J., Matthes, H., Vieira, G., Streletskiy, D. A., Schoeneich, P., Romanovsky, V. E., Lewkowicz, A. G., Abramov, A., Allard, M., Boike, J., Cable, W. L., Christiansen, H. H., Delaloye, R., Diekmann, B., Drozdov, D., Etzelmüller, B., Grosse, G., Guglielmin, M., Ingeman-Nielsen, T., Isaksen, K., Ishikawa, M., Johansson, M., Johansson, H., Joo, A., Kaverin, D., Kholodov, A., Konstantinov, P., Kröger, T., Lambiel, C., Lanckman, J.-P., Luo, D., Malkova, G., Meiklejohn, I., Moskalenko, N., Oliva, M., Phillips, M., Ramos, M., Sannel, A. B. K., Sergeev, D., Seybold, C., Skryabin, P.,
- Vasiliev, A., Wu, Q., Yoshikawa, K., Zheleznyak, M., and Lantuit, H.: Permafrost is warming at a global scale, Nat Commun, 10, 264, https://doi.org/10.1038/s41467-018-08240-4, 2019.
 - Cao, H., Gao, B., Gong, T., and Wang, B.: Analyzing Changes in Frozen Soil in the Source Region of the Yellow River Using the MODIS Land Surface Temperature Products, Remote Sensing, 13, 180, https://doi.org/10.3390/rs13020180, 2021.
- Chen, D., Zou, C., Wang, S., Li, H., and Zhang, X.: Study on spatial interpolation of the average temperature in the Yili River Valley based on DEM, Guang pu xue yu guang pu fen xi = Guang pu, 31, 1925–1929, 2011.





- Chen, F., Luo, D., Liu, L., JIn, H., and Li, C.: Variations of air freezing/thawing index during 1901—2018 in the hree-River Source Region, Journal of Glaciology and Geocryology, 43, 417–426, https://doi.org/10.7522/j.issn.1000-0240.2021.0015, 2021.
- Chen, J., Kang, S., Du, W., and Jiang, Y.: Review of Research on Observed Meteorology and Energy Balance in the Glaciated Regions of the Tibetan Plateau, Acta Meteorological Sinica, https://doi.org/10.11676/qxxb2025.20240173, 2025.
 - Cheng, G., Jiang, H., Wang, K., and Wu, Q.: Thawing Index and Freezing Index on the Embankment Surface in Permafrost Regions, Journal of Glaciology and Geocryology, 603–607, 2003.
 - F. Nelson and S. Outcalt: A Computational Method for Prediction and Regionalization of Permafrost, Arctic and alpine research, 19, 279, https://doi.org/10.2307/1551363, 1987.
- 540 Frederico Johannsen, Joao P. A. Martins, Sofia L. Ermida, and Emanuel Dutra: Evaluation of skin temperature in ECMWF reanalyses, [data set], 2019.
 - Gao, Y., Luo, D., Chen, F., Lei, W., and Jln, H.: Characteristics of the thermal regime and freeze-thaw cycles on the ground surface in permafrost regions in the Headwater Area of the Yellow River, Acta Geographica Sinica, 78, 604–619, https://doi.org/10.11821/dlxb202303007, 2023.
- 545 Hjort, J., Streletskiy, D., Doré, G., Wu, Q., Bjella, K., and Luoto, M.: Impacts of permafrost degradation on infrastructure, Nat Rev Earth Environ, 3, 24–38, https://doi.org/10.1038/s43017-021-00247-8, 2022.
 - Li, C., Zhang, W., Lai, Z., Pen, F., Chen, X., Xue, X., Wang, T., and You, quangang, Du, Heqiang: alpine steppe under different degradation degrees at the source of the Yellow Plant productivity, species diversity, soil properties, and their relationships in an River, Acta Ecologica Sinica, 1–11, 2021.
- Li, F., Hao, D., Zhu, Q., Yuan, K., Braghiere, R. K., He, L., Luo, X., Wei, S., Riley, W. J., Zeng, Y., and Chen, M.: Global impacts of vegetation clumping on regulating land surface heat fluxes, Agricultural and Forest Meteorology, 345, 109820, https://doi.org/10.1016/j.agrformet.2023.109820, 2024.
 - LI, H.: Coupling Relationship between Soil Hydrothermal Environment and Alpine Meadow Changes Based on Remote Sensing -Taking the Yellow River source area as an example, Ph.D, Qinghai Normal University, [data set], 2023.
- LI, H., Cui, Y., Wang, S., Yang, Y., and Liu, F.: A 1-km monthly surface temperature dataset of the source area of the Yellow River (1981-2020), Figshare [data set], https://doi.org/10.6084/m9.figshare.29261540, 2025a.
 - LI, H., Cui, Y., Wang, S., Yang, Y., and Liu, F.: A 1-km resolution annual freeze-thaw index dataset of the source area of the Yellow River (1981-2020, Figshare [data set], https://doi.org/10.6084/m9.figshare.29261555, 2025b.
- Li, M., Du, J., Li, W., Li, R., Wu, S., and Wang, S.: Global vegetation change and its relationship with precipitation and temperature based on GLASS-LAI in 1982-2015, SCIENTIA GEOGRAPHICA SINICA, 40, 823–832, https://doi.org/10.13249/j.cnki.sgs.2020.05.017, 2020.
 - Li, X., Zhang, Y., Yan, H., and Salahou, M. K.: Watershed-level spatial pattern of degraded alpine meadow and its key influencing factors in the Yellow River Source Zone of West China, Ecological Indicators, 146, 109865, https://doi.org/10.1016/j.ecolind.2023.109865, 2023.





- Lin, C. and Chang, X.: Spatio-Temporal Variations of Surface Temperature Lapse Rate on Qilian Mountains, Advances in Geosciences, 08, 691–698, https://doi.org/10.12677/AG.2018.83073, 2018.
 - Liu, Q. G. and Huang, Y. F.: Spatial and Temporal Changes and Driving Factors of Desertification in the Source Region of the Yellow River, China, NEPT, 19, 1435–1442, https://doi.org/10.46488/NEPT.2020.v19i04.009, 2020.
- Liu, W., Xie, C., Zhao, L., Wu, T., Wang, W., Zhang, Y., Yang, G., Zhu, X., and Yue, G.: Dynamic changes in lakes in the Hoh Xil region before and after the 2011 outburst of Zonag Lake, J. Mt. Sci., 16, 1098–1110, https://doi.org/10.1007/s11629-018-5085-0, 2019.
 - Mo, X., Liu, S., and Hu, S.: Co-evolution of climate-vegetation-hydrology and its mechanisms in the source region of Yellow River, Acta Geographica Sinica, 77, 1730–1744, https://doi.org/10.11821/dlxb202207011, 2022.
 - Muñoz-Sabater, J., Dutra, E., Agustí-Panareda, A., Albergel, C., Arduini, G., Balsamo, G., Boussetta, S., Choulga, M.,
- Harrigan, S., Hersbach, H., Martens, B., Miralles, D. G., Piles, M., Rodríguez-Fernández, N. J., Zsoter, E., Buontempo, C., and Thépaut, J.-N.: ERA5-Land: a state-of-the-art global reanalysis dataset for land applications, Earth Syst. Sci. Data, 13, 4349–4383, https://doi.org/10.5194/essd-13-4349-2021, 2021.
 - Obu, J., Westermann, S., Bartsch, A., Berdnikov, N., Christiansen, H. H., Dashtseren, A., Delaloye, R., Elberling, B., Etzelmüller, B., Kholodov, A., Khomutov, A., Kääb, A., Leibman, M. O., Lewkowicz, A. G., Panda, S. K., Romanovsky, V.,
- Way, R. G., Westergaard-Nielsen, A., Wu, T., Yamkhin, J., and Zou, D.: Northern Hemisphere permafrost map based on TTOP modelling for 2000–2016 at 1 km2 scale, Earth-Science Reviews, 193, 299–316, https://doi.org/10.1016/j.earscirev.2019.04.023, 2019.
 - Peng, X., Zhang, T., Liu, Y., and Luo, J.: Past and Projected Freezing/Thawing Indices in the Northern Hemisphere, Journal of Applied Meteorology and Climatology, 58, 495–510, https://doi.org/10.1175/JAMC-D-18-0266.1, 2019.
- Ran, Y., Cheng, G., Dong, Y., Hjort, J., Lovecraft, A. L., Kang, S., Tan, M., and Li, X.: Permafrost degradation increases risk and large future costs of infrastructure on the Third Pole, Communications Earth & Environment, 3, https://doi.org/10.1038/s43247-022-00568-6, 2022.
 - Shen, M., Piao, S., Jeong, S.-J., Zhou, L., Zeng, Z., Ciais, P., Chen, D., Huang, M., Jin, C.-S., Li, L. Z. X., Li, Y., Myneni, R. B., Yang, K., Zhang, G., Zhang, Y., and Yao, T.: Evaporative cooling over the Tibetan Plateau induced by vegetation growth,
- 590 Proceedings of the National Academy of Sciences, 112, 9299–9304, https://doi.org/10.1073/pnas.1504418112, 2015.
 - Wang, R., Zhu, Q., and Ma, H.: Changes in freezing and thawing indices over the source region of the Yellow River from 1980 to 2014, J. For. Res., 30, 257–268, https://doi.org/10.1007/s11676-017-0589-y, 2019a.
 - Wang, X., Chen, R., Han, C., Yang, Y., Liu, J., Liu, Z., and Song, Y.: Response of frozen ground under climate change in the Qilian Mountains, China, Quaternary International, 523, 10–15, https://doi.org/10.1016/j.quaint.2019.06.006, 2019b.
- Wu, H., Wu, H., Wang, Y., LI, H., Tian, F., Zhou, K., Qi, Z., Zhang, Y., Zhang, Q., and Zhang, X.: Analysis of Himalayan marmot distribution and plague risk in Qinghai province of China using the "3S" technology, Sci Rep, 13, 1924, https://doi.org/10.1038/s41598-023-28414-5, 2023.



600



Wu, T., Wang, Q., Zhao, L., Batkhishig, O., and Watanabe, M.: Observed trends in surface freezing/thawing index over the period 1987–2005 in Mongolia, Cold Regions Science and Technology, https://doi.org/10.1016/j.coldregions.2011.07.003, 2011.

- Yao, T., Qin, D., Shen, Y., Zhao, L., and Lu, A.: Cryospheric changes and their impacts on regional water cycle and ecological conditions in the Qinghai-Tibetan Plateau, Chinese Journal of Nature, 35, 179–186, 2013.
- Zhang, M., Li, R., Pei, W., Zhou, Y., Li, G., and Yang, S.: Permafrost Degradation Risk Evaluation in the Qinghai-Tibet Plateau Under Climate Change Based on Machine Learning Models, J. Geophys. Res. Atmos., 129, e2023JD039611, https://doi.org/10.1029/2023JD039611, 2024.
 - Zhang, Y., Liu, L., Bai, W., Sheng, Z., Yan, J., Ding, M., Li, S., and Zhen, D.: Grassland Degradation in the Source Region of the Yellow River, Acta Geographica Sinica, 61, 3–14, 2006.
 - Zhou, H., Zhao, X., Wen, J., Chen, Z., Yao, B., Yang, Y., Xu, W., and Duan, J.: The characteristics of soil and vegetation of degraded alpine steppe in the Yellow River source area, ACTA PRATACULTURAE SINICA, 21, 1–11, 2012.
- Zhou, H., Zhao, X., Tang, Y., Gu, S., and Zhou, L.: Alpine grassland degradation and its control in the source region of the Yangtze and Yellow Rivers, China, Grassland Science, 51, 191–203, https://doi.org/10.1111/j.1744-697X.2005.00028.x, 2005.